Journal of Biomedical Materials Research Part B: Applied Biomaterials

Early View (Articles online in advance of print)
Published Online: 5 Feb 2007

Injectable nanocrystalline hydroxyapatite paste for bone substitution: *In vivo* analysis of biocompatibility and vascularization

Matthias W. Laschke [1 *], Kristina Witt [1], Tim Pohlemann [2], Michael D. Menger [1]

[1]Institute for Clinical and Experimental Surgery, University of Saarland, 66421 Homburg/Saar, Germany
[2]Department of Trauma, Hand and Reconstructive Surgery, University of Saarland, 66421 Homburg/Saar, Germany
email: Matthias W. Laschke (matthias.laschke@uniklinik-saarland.de)
[*]Correspondence to Matthias W. Laschke, Institute for Clinical and Experimental Surgery, University of Saarland, 66421 Homburg/Saar, Germany

Funded by:
- aap Biomaterials GmbH & Co. KG, Dieburg, Germany

KEYWORDS
Ostim® • hydroxyapatite • biocompatibility • angiogenesis • dorsal skinfold chamber

ABSTRACT

The nanocrystalline hydroxyapatite paste Ostim® represents a fully degradable synthetic bone substitute for the filling of bone defects. Herein, we investigated *in vivo* the inflammatory and angiogenic host tissue response to this biomaterial after implantation. For this purpose, Ostim was implanted into the dorsal skinfold chambers of Syrian golden hamsters. The hydroxyapatite ceramic Cerabone® and isogeneic transplanted cancellous bone served as controls. Angiogenesis, microhemodynamics, microvascular permeability, and leukocyte-endothelial cell interaction of the host tissue were analyzed over 2 weeks using intravital fluorescence microscopy. Ostim exhibited good biocompatibility comparable to that of Cerabone and cancellous bone, as indicated by a lack of venular leukocyte activation after implantation. Cancellous bone induced a more pronounced angiogenic response and an increased microvessel density when compared with the synthetic bone substitutes. In contrast to Cerabone, however, Ostim showed a guided neovascularization directed toward areas of degradation. Histology confirmed the ingrowth of proliferating vascularized tissue into the hydroxyapatite paste at sites of degradation, while the hydroxyapatite ceramic was not pierced by new microvessels. Thus, Ostim represents an injectable synthetic bone substitute, which may optimize the conditions for the formation of new bone at sites of bone defects by supporting a guided vascularization during biodegradation. © 2007 Wiley Periodicals, Inc. J Biomed Mater Res Part B: Appl Biomater 2007

Received: 27 June 2006; Revised: 27 September 2006; Accepted: 7 November 2006
DIGITAL OBJECT IDENTIFIER (DOI)

10.1002/jbm.b.30755 About DOI
ARTICLE TEXT

INTRODUCTION

Reconstruction of bone defects due to fractures or resection of benign tumors and bone cysts represents a daily challenge in traumatology, orthopaedics, and neurosurgery. Correspondingly, a large variety of different methods of bone substitution has been investigated during the last decades.

Presently, the transplantation of freshly isolated autologous cancellous bone from the iliac crest is still considered the golden standard in bone repair, because it guarantees optimal osteogenesis, osteoinduction, and osteoconduction.[1] However, this approach also bears some substantial drawbacks. In some cases, the amount of isolated bone material is not sufficient to completely fill larger bone defects. Moreover, the overall surgical procedure is longer due to the isolation of the cancellous bone, resulting in increased costs for the health care system. Additionally, harvesting of bone autografts can be associated with several complications such as blood loss, haematoma formation, fracture, nerve injury, infection, cosmetic defects, and chronic pain at the donor site.[2-5] Alternatively, allografts may serve as bone substitutes, however, they raise concerns of immunorejection and transmission of infectious diseases such as HIV and hepatitis C. [1]

In order to avoid these disadvantages, a broad spectrum of biomaterials serving as synthetic bone substitutes has been developed during

the last years. Especially, calcium phosphate ceramics, such as hydroxyapatite, are increasingly introduced in clinical practice because of their good biocompatibility and bioactivity.[6] They are available as powders, granules, or blocks. However, these pharmaceutical forms are awkward when bone defects are not easily accessible or when a cavity should be filled homogeneously with the biomaterial. Thus, injectable bone substitutes, which are degradable over time, have recently been developed in order to guarantee convenient handling properties.[7-9]

Herein, we analyzed in the dorsal skinfold chamber model the injectable bone substitute Ostim® (Ostim 35®; Osartis GmbH & Co. KG, Obernburg, Germany), which contains phase pure nanosize hydroxyapatite crystals as a suspension in water. Thus, Ostim represents a high viscous, fully degradable bone substitute for the filling of bone defects with a chemical composition and a crystalline structure that is essentially identical with the mineral phase of natural bone.

Using the technique of intravital fluorescence microscopy, the implantation of Ostim into the dorsal skinfold chamber of Syrian golden hamsters allows for the repetitive assessment of inflammatory parameters such as leukocyte-endothelial cell interaction. Moreover, it enables for the study of the ingrowth of newly developing blood vessels into the biomaterial, which is an essential prerequisite for the subsequent formation of new bone. As controls, we have used hydroxyapatite ceramic (Cerabone®; Coripharm GmbH & Co. KG, Dieburg, Germany), representing one of the most frequently used synthetic bone substitutes, and isogeneic transplanted cancellous bone, the golden standard in bone repair.

MATERIALS AND METHODS

Animals

The experiments were conducted in accordance with the German legislation on protection of animals and the NIH Guidelines for the Care and Use of Laboratory Animals (NIH Publication no. 85-23 Rev. 1985), and were approved by the local governmental animal care committee.

Eight- to ten-week-old Syrian golden hamsters with a body weight of 60-80 g were used for the study. The animals were housed one per cage and had free access to tap water and standard pellet food (Altromin, Lage, Germany) throughout the experiment.

Preparation of the Dorsal Skinfold Chamber

The chamber preparation contains one layer of striated muscle, subcutis, and skin, and allows for intravital microscopic observation of the microcirculation in the awake animals over a prolonged period of time. The chamber technique and its implantation procedure have been described previously in detail.[10] Briefly, under sodium pentobarbital anesthesia (50 mg/kg body weight, i.p.), two symmetrical titanium frames were implanted on the extended dorsal skinfold of the hamsters, so that they sandwich the double layer of skin. For this, one layer of skin was completely removed in a circular area of ~15 mm in diameter, and the remaining layers (consisting of striated skin muscle and subcutaneous tissue) were covered with a removable coverslip incorporated into one of the titanium frames. After the preparation, the animals were allowed to recover from anesthesia and surgery for at least 48 h. The animals tolerated the chamber and its preparation well, as indicated by a normal feeding and sleeping habit.

Preparation and Implantation of Bone Substitutes

Ostim (Osartis GmbH & Co. KG) is a viscous paste, which contains phase pure nanosize hydroxyapatite crystals as a suspension in water [Figure 1(A)]. It is synthesized by a precipitation reaction adding orthophosphoric acid to a calcium hydroxide suspension. The chemical reaction at room temperature leads to a white suspension containing 5-6% of nanosize hydroxyapatite crystals. The suspension is then concentrated by filtration and evaporation, resulting in a solid content of 35%. The crystalline phase pure nanosize hydroxyapatite has a calcium/phosphate ratio of 1.67. The final paste of high viscosity prevents wash out effects by blood and is degraded by phagocytosis after implantation.

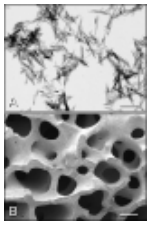

Figure 1. TEM image of Ostim® (A) and REM image of Cerabone® (B). Ostim is a viscous paste, which contains phase pure nanosize hydroxyapatite crystals as a suspension in water (A). In contrast, the granules of Cerabone are synthesized of a solid hydroxyapatite ceramic (pentacalcium hydroxide triphosphate) with a pore size of ~0.1-1.5 mm (B). Scale bars: A = 250 nm; B = 350 µm.
[Normal View 47K | Magnified View 197K]

Before implantation into the dorsal skinfold chamber, Ostim could be easily compressed in-between two microscope slides to a thickness of ~1 mm and subsequently be cut with a scalpel into small rectangular pieces (~3 × 2.5 mm^2). In contrast, the granules (diameter: ~0.5-1.6 mm) of Cerabone (Coripharm GmbH & Co. KG) are made of a solid hydroxyapatite ceramic (pentacalcium hydroxide triphosphate) with a pore size of ~0.1-1.5 mm [Figure 1(B)].

For implantation of bone substitutes, the chamber-equipped animals were immobilized in a plexiglas tube. The cover glass of the dorsal skinfold chamber was removed and comparable amounts of ~7-10 mm^3 of the nanocrystalline hydroxyapatite paste Ostim, the hydroxyapatite ceramic Cerabone (3-4 granules), or freshly isolated cancellous bone from the tibia of a donor animal were placed onto the striated muscle tissue within the center of each chamber (Figure 2).

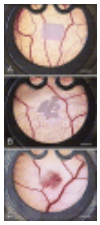

Figure 2. Dorsal skinfold chambers of Syrian golden hamsters directly after implantation of bone substitutes consisting of the nanocrystalline hydroxyapatite paste Ostim® (A), the hydroxyapatite ceramic Cerabone® (B), and isolated isogeneic cancellous bone (C). Scale bars: 1.6 mm. [Color figure can be viewed in the online issue, which is available at www.interscience.wiley.com.]
[Normal View 86K | Magnified View 351K]

Intravital Epi-Illumination Fluorescence Microscopy

For *in vivo* microscopic observation, the hamsters were again immobilized in a plexiglas tube and the dorsal skinfold preparation was attached to the microscope stage. After retrobulbary i.v. injection of 0.1 mL of 5% fluorescein isothiocyanate (FITC)-labeled dextran 150,000 (contrast enhancement by staining of blood plasma) and 0.1 mL of 0.1% rhodamine 6G (Sigma, Deisenhofen, Germany) (direct staining of leukocytes), intravital fluorescence microscopy was performed using a modified Leitz Orthoplan microscope with a 100-W mercury lamp attached to a Ploemo-Pak illuminator with blue, green, and ultraviolet filter blocks (Leitz, Wetzlar, Germany) for epi-illumination. Images were recorded by a charge-coupled device video camera (CF8/1 FMC; Kappa GmbH, Gleichen, Germany) and transferred to a video system for off-line evaluation. With the use of 4×, 6.3×, 10×, and 20× long-distance objectives (Leitz), magnifications of 86×, 136×, 216×, and 432× were achieved on a 14 in. video screen (PVM 1444; Sony, Tokyo, Japan).

Microcirculatory Analysis

Quantitative off-line analysis of the videotapes was performed by means of the computer-assisted image analysis system CapImage (Zeintl, Heidelberg, Germany). Leukocyte-endothelial cell interaction, microhemodynamics, and macromolecular leakage were assessed at a magnification of 432× in four different microvascular regions of interest (ROIs) in the border zone of the implants. In each ROI, 1-3 postcapillary or collecting venules (inner diameter: ~30-40 μm) were selected for measurements.

Leukocytes were stained *in vivo* with the fluorescent dye rhodamine 6G and classified according to their interaction with the vascular endothelium as adherent, rolling, or free-flowing cells, as described previously.[11] Adherent leukocytes were defined in each vessel segment as cells that did not move or detach from the endothelial lining within a specified observation period of 20 s, and are given as number of cells per square millimeter of endothelial surface, calculated from the diameter and length of the vessel segment studied, assuming a cylindrical vessel geometry. Rolling leukocytes were defined as cells moving with a velocity less than two-fifths of the centerline velocity, and are given as number of cells per minute, passing a reference point within the microvessel.

Diameters, centerline velocity, volumetric blood flow, and wall shear rate were determined in those venules in which leukocyte-endothelial cell interaction was analyzed. Diameters (d) were measured in micrometers perpendicularly to the vessel path. Centerline velocity (v) was analyzed by the computer-assisted image analysis system using the line shift method. Volumetric blood flow was calculated by Q (pL/s) = $\pi(d/2)^2(v/1.6)$, where 1.6 represents the Baker-Wayland factor[12] to correct for the parabolic velocity profile in microvessels with diameters >20 μm. Wall shear (y) rate was calculated based on the Newtonian definition: $y = 8v/d$.

Macromolecular leakage served as a parameter of microvascular permeability and, thus, endothelial integrity. For analysis, the macromolecular fluorescent dye FITC-labeled dextran 150,000 was injected intravenously, and grey levels in the tissue directly adjacent to the venular vessel wall (E_1) and in the marginal cell free plasma layer within the vessel (E_2) were determined densitometrically. Extravasation (E) was then calculated as $E = E_1/E_2$.

Angiogenesis was analyzed at a magnification of 216× in eight different microvascular ROIs in the border zone and the center of the implants. ROIs were defined as "angiogenesis positive," when signs of blood vessel development, that is capillary sprouts or newly formed microvessels growing into the implants, could be identified. Additionally, more detailed information about the extent of vascular ingrowth into the different ROIs of the implants was provided by the quantitative assessment of the microvessel density, that is the length of newly formed blood vessels per area of observation, given in cm/cm^2.

Experimental Protocol

For intravital fluorescence microscopy, dorsal skinfold chambers were prepared in a total of 21 Syrian golden hamsters. Subsequently, the bone substitutes Ostim ($n = 7$), Cerabone ($n = 7$), or isogeneic cancellous bone ($n = 7$) were implanted into the skinfold chambers, taking care to avoid contamination, mechanical irritation, or damage of the chamber. The macroscopic appearance of the skinfold chamber preparations and the bone substitutes were documented daily. Intravital fluorescence microscopic assessment of angiogenesis, microhemodynamics, leukocyte-endothelial cell interaction, and macromolecular leakage was performed before (baseline) as well as 20 min, 3, 6, 10, and 14 days after implantation. At the end of the *in vivo* experiments, that is at day 14, the animals were sacrificed by an overdose of the anesthetic, and histological examinations of the dorsal skinfold chamber preparations were performed.

Histology and Immunohistochemistry

For light microscopy, formalin-fixed specimens of the dorsal skinfold chambers were embedded in paraffin at day 14 after transplantation. Four-micrometer-thick sections were cut and stained with hematoxylin and eosin according to standard procedures. For immunohistochemical detection of proliferating cells within the newly developing granulation tissue surrounding the implanted bone substitutes, proliferating cell nuclear antigen (PCNA) staining was performed by a mouse monoclonal anti-PCNA antibody as primary antibody (1:50; Dako Cytomation). This was followed by a HRP-conjugated goat anti-mouse antibody (1:200; Amersham Biosciences). 3,3′ Diaminobenzidine was used as chromogen. The sections were counter-stained with hemalaun and examined by light microscopy (BX60; Olympus, Hamburg, Germany).

Electron Microscopy

The material architecture of the synthetic bone substitutes Ostim and Cerabone was studied by transmission electron microscopy (TEM) or reflection electron microscopy (REM), respectively. For this purpose, the hydroxyapatite paste Ostim was diluted with water to a concentration of 0.01-0.02%, sprayed on a coated microscope grid, and dried. Subsequently, the biomaterial was examined in a transmission electron microscope at 10-15 kV (Philips CM 12 STEM®; FEI Company, Eindhoven, The Netherlands). For REM of Cerabone, the fractured surface of a Cerabone block was sputtered with platinum and the surface topography was imaged at 5 kV (Philips ESEM-FEG; Philips, Hamburg, Germany).

Statistics

After testing the data for normal distribution and equal variance, differences between groups were analyzed by ANOVA, followed by the Dunnett test for multiple comparisons. To test for time effects, ANOVA for repeated measures was applied. This was followed by the paired Student's t test, including correction of the α-error according to Bonferroni probabilities for repeated measurements (SigmaStat; Jandel Corporation, San Rafael, CA). All values are expressed as means ± SEM. Statistical significance was accepted for a value of $p < 0.05$.

RESULTS

Inflammation

Under baseline conditions, numbers of adherent leukocytes in postcapillary and collecting venules of the dorsal skinfold chamber ranged from 90 to 150 cells/mm^2 in the three experimental groups and did not markedly increase after implantation of the bone substitutes (Table I; Figure 2). Correspondingly, numbers of rolling leukocytes ranged from 20 to 31 cells/min during the experiment without any significant differences over time and between the three groups (Table I). The lack of activation of leukocytes after implantation indicates an adequate biocompatibility of Ostim (Figure 3), comparable to that of Cerabone and cancellous bone.

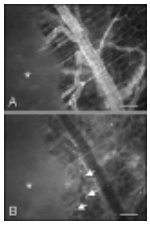

Figure 3. Intravital fluorescence microscopy of the microcirculation within the border zone of an Ostim® implant (asterisk) at day 6 after transfer onto the striated muscle tissue of the dorsal skinfold chamber. Note that there are only a few activated leukocytes adhering at the endothelium of postcapillary venules (arrows), indicating an adequate biocompatibility of the bone substitute. (A) Blue-light epi-illumination with contrast enhancement by 5% FITC-labeled dextran 150,000 i.v. for visualization of the microvasculature. (B) Green-light epi-illumination for visualization of rhodamine 6G-stained leukocytes. Scale bars: 170 µm.
[Normal View 41K | Magnified View 162K]

Table I. Adherent and Rolling Leukocytes in Postcapillary and Collecting Venules Within the Border Zones of Ostim®, Cerabone®, and Cancellous Bone Before (BL, Baseline) as well as 20 min, 3, 6, 10, and 14 Days After Implantation Into the Dorsal Skinfold Chamber of Syrian Golden Hamsters

	Adherent Leukocytes (cells/mm^2)			Rolling Leukocytes (cells/min)		
	Ostim	Cerabone	Cancellous Bone	Ostim	Cerabone	Cancellous Bone
BL	94.4 ± 12.1	120.1 ± 20.7	147.1 ± 33.5	20.9 ± 1.2	24.1 ± 2.6	27.3 ± 3.1
20 min	147.3 ± 27.0	197.6 ± 36.5	182.1 ± 25.3	23.4 ± 4.2	17.0 ± 2.9	20.2 ± 1.5
3 days	122.7 ± 18.8	85.9 ± 11.9	102.5 ± 17.7	26.6 ± 3.9	23.1 ± 2.3	21.0 ± 2.7
6 days	127.2 ± 32.8	103.6 ± 18.0	97.4 ± 18.2	24.3 ± 3.5	31.3 ± 4.7	28.0 ± 4.3
10 days	90.9 ± 12.3	77.6 ± 7.3	80.1 ± 13.0	31.3 ± 6.1	22.8 ± 3.0	20.8 ± 2.4
14 days	131.9 ± 19.3$^{\#}$	94.5 ± 13.7	60.7 ± 8.3^{+}	29.2 ± 5.9	25.1 ± 2.3	23.1 ± 3.7

Data are given as mean ± SEM.
$^{+}$ $p < 0.05$ versus BL.
$^{\#}$ $p < 0.05$ versus cancellous bone at corresponding time points.

Macromolecular leakage from the microvasculature of the border zones of the bone substitutes showed a progressive increase throughout the observation period (Figure 4) due to an altered integrity of the venular endothelial lining cells. Interestingly, this was most pronounced in dorsal skinfold chambers with implanted cancellous bone revealing a macromolecular leakage of 0.66 ± 0.04 at day 14, which was significantly higher compared with that observed in Ostim implants (0.50 ± 0.05; $p < 0.05$) (Figure 4).

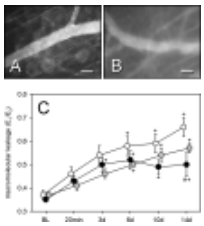

Figure 4. (A,B) Intravital fluorescence microscopy of postcapillary venules of the dorsal skinfold chamber preparation before implantation of cancellous bone (A, baseline) and at day 14 after implantation (B). Fourteen days after implantation of cancellous bone, extravasation of the intravenously injected macromolecular fluorescent dye FITC-labeled dextran 150,000 is increased, indicating an altered integrity of the endothelial cells lining the vessel walls. Blue-light epi-illumination with contrast enhancement by 5% FITC-labeled dextran 150,000 i.v. Scale bars: 50 µm. (C) Macromolecular leakage as a parameter of microvascular permeability of postcapillary and collecting venules within ROIs of the border zones of Ostim® (black circles), Cerabone® (grey circles), and cancellous bone (white circles) before (BL, baseline) as well as 20 min, 3, 6, 10, and 14 days after implantation into the dorsal skinfold chamber of Syrian golden hamsters. Mean ± SEM. $^{+}p < 0.05$ versus BL; $^{\#}p < 0.05$ versus cancellous bone at corresponding time points.
[Normal View 28K | Magnified View 79K]

Microhemodynamics

Analysis of microhemodynamics revealed constant venular diameters of 30-40 µm without any differences between the groups (Table II). Furthermore, centerline velocity, volumetric blood flow, and shear rates of venules in direct vicinity to the implants did not change during the 14-day observation period and were comparable in all experimental groups (Table II).

Table II. Diameter, Centerline Velocity, Volumetric Blood Flow, and Shear Rate of Postcapillary and Collecting Venules Within the Border Zones of Ostim®, Cerabone®, and Cancellous Bone Before (BL, Baseline) as well as 20 min, 3, 6, 10, and 14 days After Implantation Into the Dorsal Skinfold Chamber of Syrian Golden Hamsters

Diameter (µm)	Centerline Velocity (µm/s)	Volumetric Blood Flow (pL/s)	Shear Rate (s^{-1})

	Ostim	Cerabone	Cancellous Bone	Ostim	Cerabone	Cancellous Bone	Ostim	Cerabone	Cancellous Bone	Ostim	Cerabone	Cancellous Bone
BL	34.0 ± 1.8	31.1 ± 1.4	33.1 ± 1.5	278 ± 18	262 ± 41	240 ± 43	161 ± 20	125 ± 23	130 ± 26	66.1 ± 4.5	68.8 ± 11.4	58.4 ± 10.6
20 min	37.8 ± 1.6	34.2 ± 2.3	37.5 ± 2.1	339 ± 59	317 ± 53	263 ± 39	238 ± 43	185 ± 36	180 ± 29	72.8 ± 13.7	76.6 ± 13.9	58.1 ± 10.2
3 days	38.6 ± 2.6	33.1 ± 2.3	31.9 ± 1.5	330 ± 49	257 ± 44	275 ± 35	267 ± 69	158 ± 39	144 ± 26	67.4 ± 7.6	60.1 ± 8.8	68.2 ± 7.0
6 days	38.9 ± 2.1	36.8 ± 1.5	38.6 ± 3.3	381 ± 38	375 ± 49	331 ± 41	287 ± 37	258 ± 47	265 ± 63	79.4 ± 10.1	81.5 ± 10.7	69.7 ± 9.8
10 days	36.9 ± 2.3	31.2 ± 1.1	34.9 ± 1.4	222 ± 34	325 ± 61	320 ± 42	155 ± 30	163 ± 42	198 ± 36	48.5 ± 7.5	82.2 ± 13.4	72.8 ± 8.8
14 days	31.8 ± 1.6	35.5 ± 2.0	38.9 ± 2.7	240 ± 26	351 ± 58	363 ± 49	124 ± 21	235 ± 63	294 ± 66	60.7 ± 6.2	78.8 ± 11.2	74.7 ± 8.5

Data are given as mean ± SEM.

Angiogenesis and Material Incorporation

First signs of angiogenesis could be observed within the border zones of the bone substitutes at day 3 after implantation. These were characterized by formation of capillary buds and protrusion of capillary sprouts, which originated primarily from venular segments of the striated muscle capillaries and postcapillary venules of the host tissue [Figures 5 and 6(A)]. During the following days, these sprouts developed to newly formed blood vessels, ingrowing into the central areas of the bone substitutes [Figures 5 and 6(B)]. Of interest, the angiogenic process was markedly accelerated in cancellous bone, in which 100% of the analyzed ROIs in the center of the implants were angiogenesis positive at days 10 and 14. At this time point, substantial areas in the center of Ostim and Cerabone implants still lacked newly formed blood vessels [Figures 5 and 6(B)]. In addition, the microvessel density of newly developing microvascular networks in the border and the center of cancellous bone was significantly higher ($p < 0.05$) at days 10 and 14 when compared with that of Ostim and Cerabone implants [Figure 6(C,D)]. However, although the overall microvessel density of Ostim was lower compared with cancellous bone, the degradable material exhibited a guided neovascularization, which was directed toward areas of degradation (Figure 7).

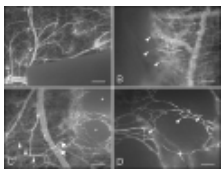

Figure 5. Intravital fluorescence microscopy of Ostim® at 20 min (A) as well as day 3 (B) and day 14 (C,D) after implantation into the dorsal skinfold chamber of a Syrian golden hamster. At day 3, first signs of angiogenesis can be observed in the border zone of the implant, characterized by capillary sprouts (B, arrow heads) ingrowing into the bone substitute. At day 14, the border zone of the implant is already well vascularized (C), while areas in the center of the implant still lack newly formed blood vessels (C, asterisks). However, higher magnification of the bone substitute demonstrates that the angiogenic process continues, as indicated by capillary sprouts (D, arrow heads) ingrowing into avascular areas of the center of the implant (D). Note that the newly formed microvascular network of the implant is drained by postcapillary vessels (C, arrows), which connect to the parallelly arranged striated muscle capillaries (C, arrow heads) of the skinfold chamber. Blue light epi-illumination with contrast enhancement by 5% FITC-labeled dextran 150,000 i.v. Scale bars: A = 270 µm; B = 105 µm; C = 170 µm; D = 105 µm.
[Normal View 73K | Magnified View 303K]

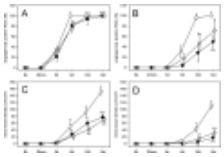

Figure 6. (A,B) Time course of angiogenesis after implantation of Ostim® (black circles), Cerabone® (grey circles), and cancellous bone (white circles) expressed as percentage of "angiogenesis positive" regions of interest (ROIs) within the border zone (A) and the center (B) of the implants before (BL, baseline) as well as 20 min, 3, 6, 10, and 14 days after implantation into the dorsal skinfold chamber of Syrian golden hamsters. ROIs were defined as "angiogenesis positive," when signs of blood vessel development, that is capillary buds and sprouts or newly formed microvessels, could be identified. (C,D) Quantitative assessment of the microvessel density, given as cm/cm^2, in ROIs within the border zone (C) and the center (D) of Ostim (black circles), Cerabone (grey circles), and cancellous bone (white circles) before (BL, baseline) as well as 20 min, 3, 6, 10, and 14 days after implantation into the dorsal skinfold chamber of Syrian golden hamsters. Mean ± SEM. $^{+}p < 0.05$ versus BL; $^{\#}p < 0.05$ versus cancellous bone at corresponding time points.
[Normal View 47K | Magnified View 131K]

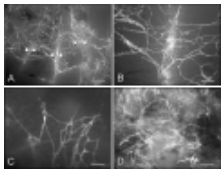

Figure 7. Intravital fluorescence microscopy of Ostim® (A,B), Cerabone® (C), and cancellous bone (D) at day 14 after implantation into the dorsal skinfold chamber of a Syrian golden hamster. The lower magnification of Ostim (A) displays areas of material degradation (arrows). The higher magnification of these areas (B) reveals a dense ingrowth of newly formed blood vessels through the biomaterial, creating microvascular networks surrounding the remaining nondegraded Ostim fragments. In contrast to Ostim, capillaries grow only over the surface of Cerabone (C), while the granulation tissue surrounding the fragments of isolated cancellous bone is pierced by many blood vessels (D). Blue light epi-illumination with contrast enhancement by 5% FITC-labeled dextran 150,000 i.v. Scale bars: A = 270 µm; B-D = 105 µm.
[Normal View 78K | Magnified View 310K]

Histology of the dorsal skinfold chamber preparations at day 14 revealed the formation of a vascularized granulation tissue surrounding the bone substitutes. Of interest, this newly formed tissue did not show infiltration of inflammatory cells (Figure 8), indicating an adequate biocompatibility of the implanted materials. Because Ostim is a fully degradable nanocrystalline hydroxyapatite paste, newly developing blood vessels could also directly invade the biomaterial in areas of degradation, which was not observed in hydroxyapatite ceramic Cerabone [Figure 8(A-D)]. Corresponding to our intravital microscopic findings, implanted cancellous bone exhibited granulation tissue with a higher blood vessel density [Figure 8(E,F)]. Immunohistochemical staining of PCNA revealed a high proliferating activity of the granulation tissue in all three groups (Figure 9). Detailed analysis indicated that almost all cells surrounding the cancellous bone were PCNA-positive, indicating an accelerated incorporation of cancellous bone into the host tissue when compared with the synthetic bone substitutes (Figure 9).

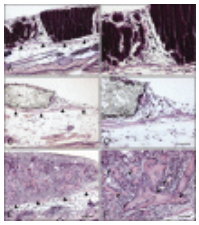

Figure 8. Hematoxylin-eosin stained cross sections of Ostim® (A), Cerabone® (C), and cancellous bone (E) at day 14 after implantation onto the striated muscle tissue (arrows) of the dorsal skinfold chamber. Higher magnification reveals the formation of granulation tissue with newly developed blood vessels (arrow heads) surrounding the Ostim (B), Cerabone (D), and cancellous bone implants (F). In contrast to Cerabone, Ostim exhibits areas of degradation (asterisks), where blood vessels can directly invade the biomaterial (A,B). Cancellous bone is surrounded by a richly vascularized granulation tissue with an increased microvessel density and a higher cellular content, when compared with the synthetic bone substitutes Ostim and Cerabone. Scale bars: A,C = 110 µm; E = 170 µm; B,D,F = 55 µm. [Color figure can be viewed in the online issue, which is available at www.interscience.wiley.com.]
[Normal View 190K | Magnified View 809K]

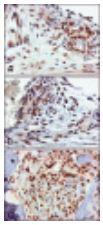

Figure 9. Immunohistochemical detection of PCNA-positive cells within the granulation tissue surrounding Ostim® (A, asterisk), Cerabone® (B, asterisk), and cancellous bone (C, asterisk) at day 14 after implantation into the dorsal skinfold chamber. Note that in the major fraction of cells surrounding Ostim and Cerabone positive PCNA staining can be observed (A,B). In cancellous bone almost all cells surrounding the implant show proliferative activity (C). Scale bars: A-C = 25 µm. [Color figure can be viewed in the online issue, which is available at www.interscience.wiley.com.]
[Normal View 88K | Magnified View 377K]

DISCUSSION

In the present study, we have analyzed *in vivo* the biocompatibility and incorporation of the injectable nanocrystalline hydroxyapatite paste Ostim during the first 14 days after implantation. We could demonstrate that Ostim does not induce an acute inflammatory response of the surrounding host tissue, as indicated by a lack of leukocyte activation in blood vessels located in the close vicinity of the implant. Accordingly, there was no infiltration of the biomaterial by inflammatory cells. Moreover, microhemodynamic parameters of the host microvasculature were not deteriorated after implantation of the biomaterial. Thus, the biocompatibility of Ostim was comparable to that of hydroxyapatite ceramic, which presently represents one of the most commonly used synthetic bone substitutes in clinical practice. [13][14]

The good biocompatibility of Ostim and Cerabone may be attributed to the fact that both bone substitutes are composed of hydroxyapatite, which is similar to the crystalline phase of natural bone.[15] However, in contrast to the hydroxyapatite ceramic Cerabone, Ostim offers better handling properties, because it is a viscous paste, which also allows for the filling of complex bone defects that are difficult to access. Moreover, an injectable bone substitute offers the possibility of implantation by percutaneous surgery.

In the past, newly developed bone substitutes have been tested *in vivo* using numerous experimental models, most of them involving larger animals such as dogs,[16] goats,[17] or rabbits.[18] In our study, we have used the dorsal skinfold chamber model of Syrian golden hamsters, which bears the advantages of convenient handling and lower costs. Of interest, in this model, the bone substitutes are not directly implanted into a bone defect, but onto the striated muscle tissue within the chamber, guaranteeing a permanent access to the implants for continuous *in vivo* analyses. Thus, this model in combination with the technique of high resolution fluorescence microscopy allows for the repetitive investigation of vascular ingrowth into the implanted bone substitutes from the surrounding soft tissue and changes of inflammatory and microhemodynamic parameters over time. During the last years, the skinfold chamber model has already been successfully used to test the material properties of various biomaterials including prosthetic vascular grafts,[19][20] arthroplasty alloys,[21][22] surgical meshes,[23] and scaffolds for tissue engineering.[24]

Beside a good biocompatibility, synthetic bone substitutes should ensure the formation of new bone after their implantation. In fact, an optimal synthetic bone substitute is reabsorbed and replaced by vital bone over time.[25] A major prerequisite for this process is angiogenesis, that is the development of new capillaries from preexisting blood vessels. Because newly formed blood vessels transport oxygen and nutrients into the implanted bone substitute, a physiological milieu is created, which supports the ingrowth of bone cells, but also the differentiation of pluripotential stem cells from the surrounding tissue to an osteoblastic phenotype.[26][27]

In our study, both synthetic bone substitutes, Ostim and Cerabone, were able to induce angiogenesis. In contrast to the nondegradable Cerabone, however, Ostim revealed areas of degradation already at day 14 after implantation. Within these areas, vascularized granulation tissue could directly invade the biomaterial. This guided vascularization may accelerate the formation of new bone in bone defects, because osteoblasts are facilitated to migrate into these vascularized areas, where the remaining nondegraded Ostim fragments serve as a scaffold for the invading cells. In this process, the newly developing blood vessels play an important role, because it has previously been reported that endothelial cells stimulate the differentiation of preosteoblasts to osteoblasts by the expression of osteotropic growth factors, such as endothelin-1 and IGF-1.[28] Vice versa, the expression of VEGF by osteoblasts further sustains the proliferation of endothelial cells and, thus, the formation of new blood vessels.[29]

In comparison to Ostim and Cerabone, vascularization of isogeneic transplanted cancellous bone was accelerated and more pronounced, as indicated by a significantly higher microvessel density of the newly developing capillary networks. This observation is most probably due to the fact that the bone marrow surrounding the isolated cancellous bone contains a high amount of regenerative cell types, such as

stem cells or endothelial progenitor cells, and different growth factors, stimulating and accelerating the development of new blood vessels.[30][31] Correspondingly, the newly formed granulation tissue surrounding the cancellous bone exhibited a higher content of proliferating cells, indicating an accelerated incorporation of the material into the host tissue. In line with this, the macromolecular leakage as a parameter of microvascular permeability increased to highest values in dorsal skinfold chambers with implanted cancellous bone, because the angiogenic process is associated with an altered endothelial integrity of the microvasculature due to the disruption of the basal membrane and the migration of endothelial cells into the surrounding tissue.[32]

In summary, we introduce in the present study the dorsal skinfold chamber as an ideal tool to study *in vivo* the inflammatory and angiogenic response to implanted bone substitutes. Herein, we could demonstrate that the nanocrystalline hydroxyapatite paste Ostim is characterized by a good biocompatibility, which is comparable to that of hydroxyapatite ceramic and cancellous bone. In comparison to Cerabone, Ostim offers better handling properties and is degraded in a short time period after implantation, supporting the ingrowth of granulation tissue with newly formed blood vessels into the biomaterial. Accordingly, implantation of Ostim may optimize the conditions for the formation of new bone, and, thus, may accelerate and improve the healing of bone defects.

Acknowledgements

We are grateful to Janine Becker for her excellent technical assistance.

REFERENCES

1 Giannoudis PV,Dinopoulos H,Tsiridis E. Bone substitutes: An update. *Injury* 2005; **36** (Suppl 3): S20-S27. Links

2 Banwart JC,Asher MA,Hassanein RS. Iliac crest bone graft harvest donor site morbidity. A statistical evaluation. *Spine* 1995; **20**: 1055-1060. Links

3 Arrington ED,Smith WJ,Chambers HG,Bucknell AL,Davino NA. Complications of iliac crest bone graft harvesting. *Clin Orthop Relat Res* 1996; **329**: 300-309. Links

4 Seiler JG III,Johnson J. Iliac crest autogenous bone grafting: donor site complications. *J South Orthop Assoc* 2000; **9**: 91-97. Links

5 Ross N,Tacconi L,Miles JB. Heterotopic bone formation causing recurrent donor site pain following iliac crest bone harvesting. *Br J Neurosurg* 2000; **14**: 476-479. Links

6 Bloemers FW,Blokhuis TJ,Patka P,Bakker FC,Wippermann BW,Haarman HJ. Autologous bone versus calcium-phosphate ceramics in treatment of experimental bone defects. *J Biomed Mater Res B Appl Biomater* 2003; **66**: 526-531. Links

7 Grimandi G,Weiss P,Millot F,Daculsi G. In vitro evaluation of a new injectable calcium phosphate material. *J Biomed Mater Res* 1998; **39**: 660-666. Links

8 Aho AJ,Tirri T,Kukkonen J,Strandberg N,Rich J,Seppala J,Yli-Urpo A. Injectable bioactive glass/biodegradable polymer composite for bone and cartilage reconstruction: Concept and experimental outcome with thermoplastic composites of poly (ε-caprolactone-*co*-**D**,**L**-lactide) and bioactive glass S53P4. *J Mater Sci Mater Med* 2004; **15**: 1165-1173. Links

9 Thorwarth M,Schultze-Mosgau S,Kessler P,Wiltfang J,Schlegel KA. Bone regeneration in osseous defects using a resorbable nanoparticular hydroxyapatite. *J Oral Maxillofac Surg* 2005; **63**: 1626-1633. Links

10 Menger MD,Laschke MW,Vollmar B. Viewing the microcirculation through the window: Some twenty years experience with the hamster dorsal skinfold chamber. *Eur Surg Res* 2002; **34**: 83-91. Links

11 Hoffmann JN,Vollmar B,Laschke MW,Inthorn D,Schildberg FW,Menger MD. Hydroxyethyl starch (130 kD), but not crystalloid volume support, improves microcirculation during normotensive endotoxemia. *Anesthesiology* 2002; **97**: 460-470. Links

12 Baker M,Wayland H. On-line volume flow rate and velocity profile measurement for blood in microvessels. *Microvasc Res* 1974; **7**: 131-143. Links

13 Uchida A,Araki N,Shinto Y,Yoshikawa H,Kurisaki E,Ono K. The use of calcium hydroxyapatite ceramic in bone tumour surgery. *J Bone Joint Surg Br* 1990; **72**: 298-302. Links

14 Matsumine A,Myoui A,Kusuzaki K,Araki N,Seto M,Yoshikawa H,Uchida A. Calcium hydroxyapatite ceramic implants in bone tumour surgery. A long-term follow-up study. *J Bone Joint Surg Br* 2004; **86**: 719-725. Links

15 Posner AS. Crystal chemistry of bone mineral. *Physiol Rev* 1969; **49**: 760-792. Links

16 Nishikawa T,Masuno K,Tominaga K,Koyama Y,Yamada T,Takakuda K,Kikuchi M,Tanaka J,Tanaka A. Bone repair analysis in a novel biodegradable hydroxyapatite/collagen composite implanted in bone. *Implant Dent* 2005; **14**: 252-260. Links

17 Arts JJ,Gardeniers JW,Welten ML,Verdonschot N,Schreurs BW,Buma P. No negative effects of bone impaction grafting with bone and ceramic mixtures. *Clin Orthop Relat Res* 2005; **438**: 239-247. Links

18 Imaizumi H,Sakurai M,Kashimoto O,Kikawa T,Suzuki O. Comparative study on osteoconductivity by synthetic octacalcium phosphate and sintered hydroxyapatite in rabbit bone marrow. *Calcif Tissue Int* 2006; **78**: 45-54. Links

19 Menger MD,Hammersen F,Walter P,Messmer K. Neovascularization of prosthetic vascular grafts. Quantitative analysis of angiogenesis and microhemodynamics by means of intravital microscopy. *Thorac Cardiovasc Surg* 1990; **38**: 139-145. Links

20 Menger MD,Hammersen F,Messmer K. In vivo assessment of neovascularization and incorporation of prosthetic vascular biografts. *Thorac Cardiovasc Surg* 1992; **40**: 19-25. Links

21 Kraft CN,Burian B,Diedrich O,Gessmann J,Wimmer MA,Pennekamp PH. Microvascular response of striated muscle to common arthroplasty-alloys: A comparative in vivo study with CoCrMo, Ti-6Al-4V, and Ti-6Al-7Nb. *J Biomed Mater Res A* 2005; **75**: 31-40. Links

22 Pennekamp PH,Gessmann J,Diedrich O,Burian B,Wimmer MA,Frauchiger VM,Kraft CN. Short-term microvascular response of striated muscle to cp-Ti, Ti-6Al-4V, and Ti-6Al-7Nb. *J Orthop Res* 2006; **24**: 531-540. Links

23 Laschke MW,Haufel JM,Thorlacius H,Menger MD. New experimental approach to study host tissue response to surgical mesh materials in vivo. *J Biomed Mater Res A* 2005; **74**: 696-704. Links

24 Druecke D,Langer S,Lamme E,Pieper J,Ugarkovic M,Steinau HU,Homann HH. Neovascularization of poly(ether ester) block-copolymer scaffolds in vivo: Long-term investigations using intravital fluorescent microscopy. *J Biomed Mater Res A* 2004; **68**: 10-18. Links

25 Gauthier O,Khairoun I,Bosco J,Obadia L,Bourges X,Rau C,Magne D,Bouler JM,Aguado E,Daculsi G,Weiss P. Noninvasive bone replacement with a new injectable calcium phosphate biomaterial. *J Biomed Mater Res A* 2003; **66**: 47-54. Links

26 Cypher TJ,Grossman JP. Biological principles of bone graft healing. *J Foot Ankle Surg* 1996; **35**: 413-417. Links

27 Moore WR,Graves SE,Bain GI. Synthetic bone graft substitutes. *ANZ J Surg* 2001; **71**: 354-361. Links

28 Rubanyi GM,Polokoff MA. Endothelins: Molecular biology, biochemistry, pharmacology, physiology, and pathophysiology. *Pharmacol Rev* 1994; **46**: 325-415. Links

29 Deckers MM,Karperien M,van der Bent C,Yamashita T,Papapoulos SE,Lowik CW. Expression of vascular endothelial growth factors and their receptors during osteoblast differentiation. *Endocrinology* 2000; **141**: 1667-1674. Links

30 Engstrand T. Molecular biologic aspects of cartilage and bone: Potential clinical applications. *Ups J Med Sci* 2003; **108**: 25-35. Links

31 Zwaginga JJ,Doevendans P. Stem cell-derived angiogenic/vasculogenic cells: Possible therapies for tissue repair and tissue engineering. *Clin Exp Pharmacol Physiol* 2003; **30**: 900-908. Links

32 Carmeliet P. Mechanisms of angiogenesis and arteriogenesis. *Nat Med* 2000; **6**: 389-395. Links

J. Biomed. Mater. Res. Vol.9999, 9999 Pages: NA

View Normal Image View List of Images

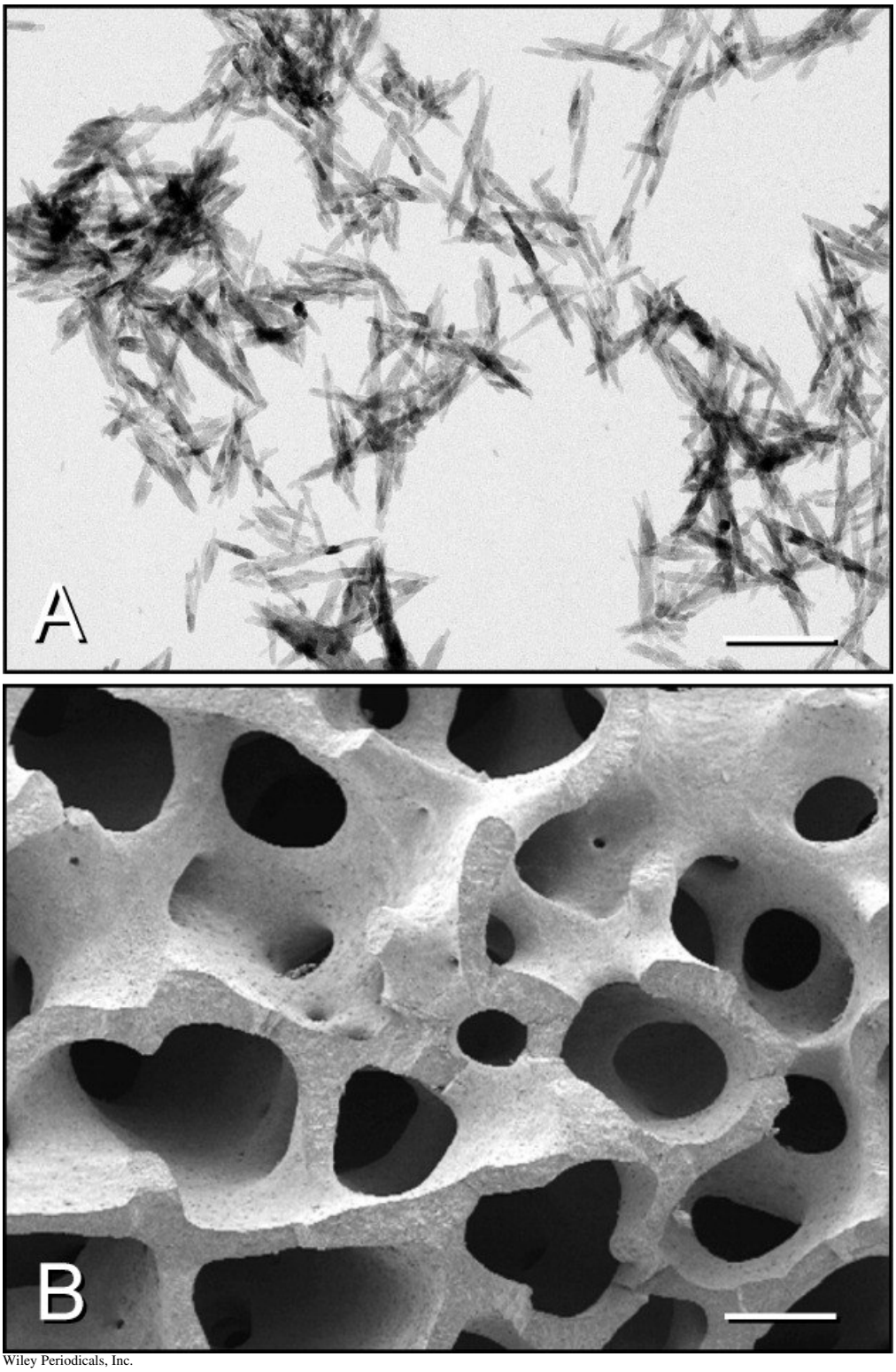

Figure 1. TEM image of Ostim® (A) and REM image of Cerabone® (B). Ostim is a viscous paste, which contains phase pure nanosize hydroxyapatite crystals as a suspension in water (A). In contrast, the granules of Cerabone are synthesized of a solid hydroxyapatite ceramic (pentacalcium hydroxide triphosphate) with a pore size of ~0.1-1.5 mm (B). Scale bars: A = 250 nm; B = 350 μm.

J. Biomed. Mater. Res. Vol.9999, 9999 Pages: NA

View Normal Image View List of Images

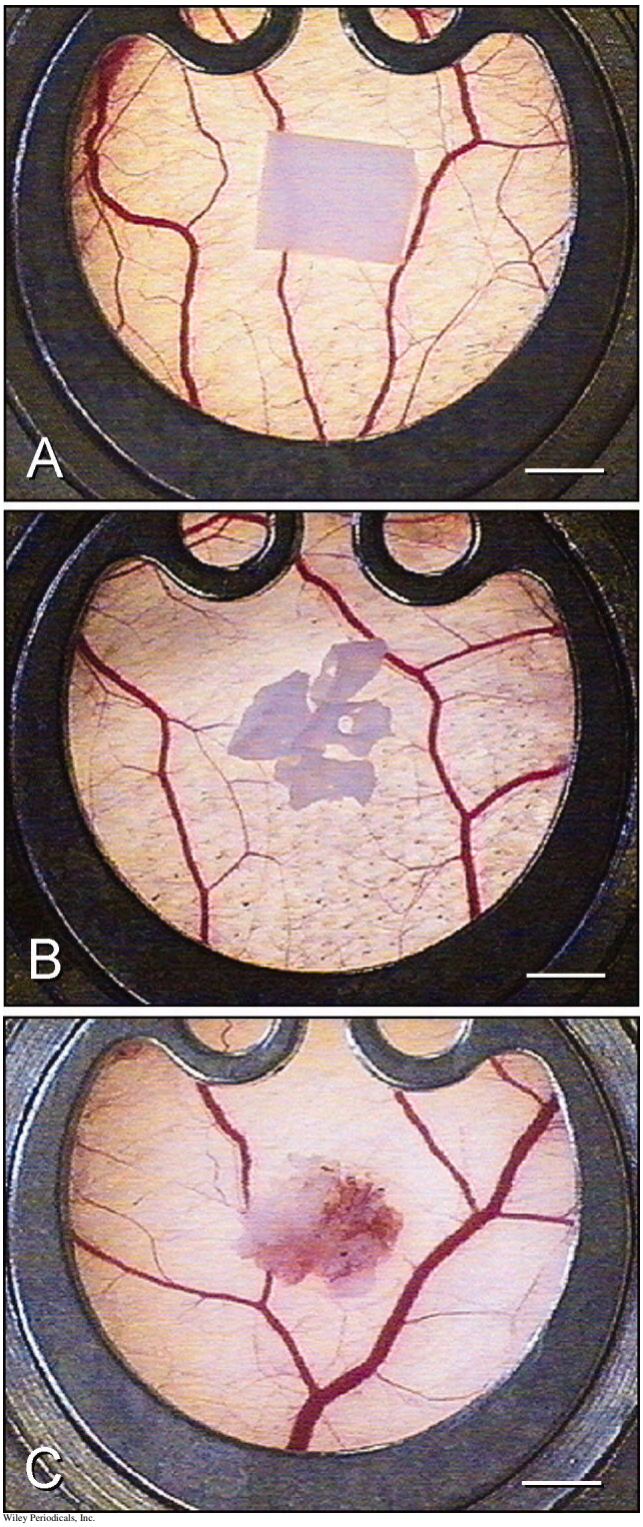

Figure 2. Dorsal skinfold chambers of Syrian golden hamsters directly after implantation of bone substitutes consisting of the nanocrystalline hydroxyapatite paste Ostim® (A), the hydroxyapatite ceramic Cerabone® (B), and isolated isogeneic cancellous bone (C). Scale bars: 1.6 mm. [Color figure can be viewed in the online issue, which is available at www.interscience.wiley.com.]

J. Biomed. Mater. Res. Vol.9999, 9999 Pages: NA

View Normal Image View List of Images

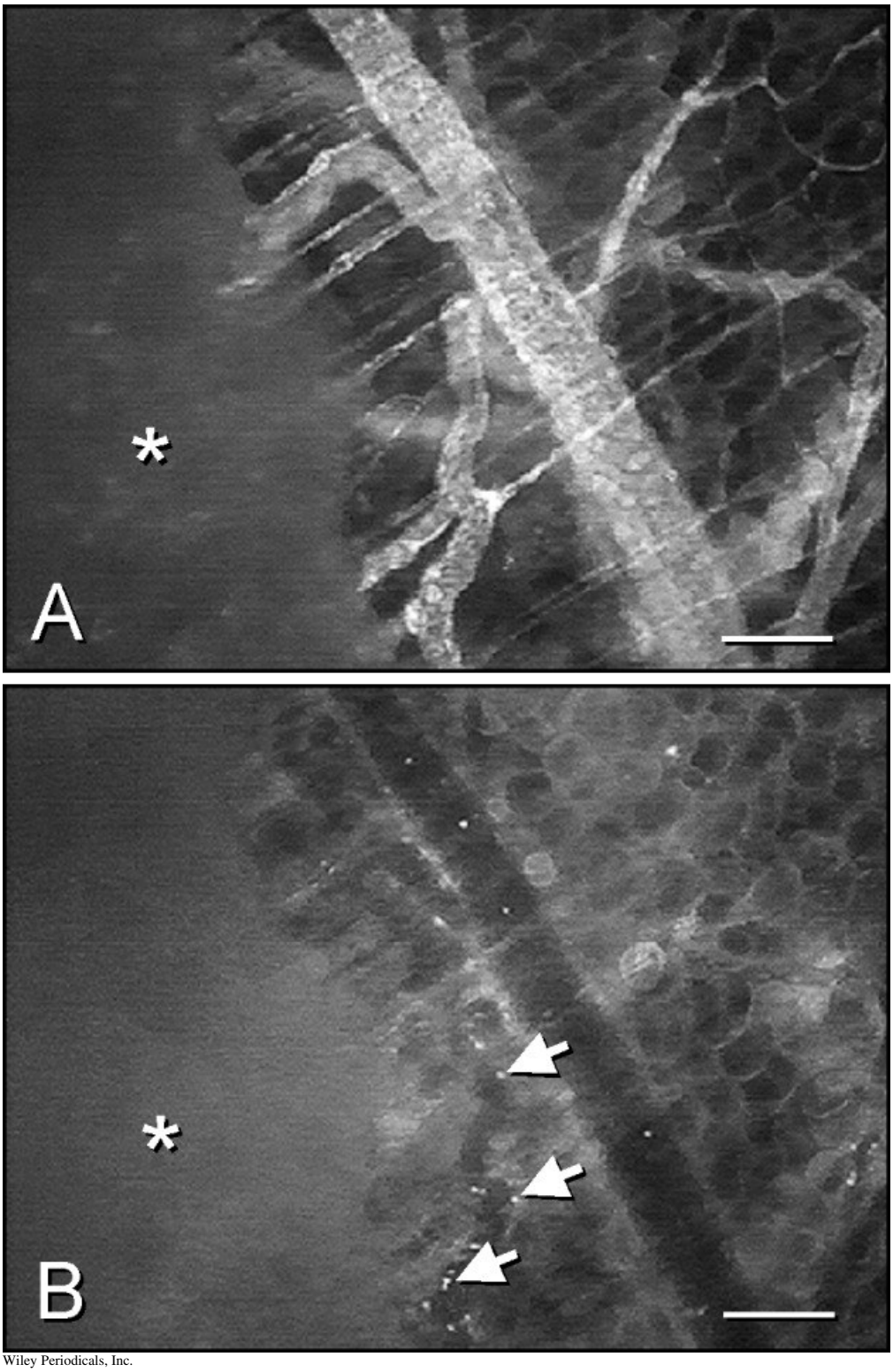

Figure 3. Intravital fluorescence microscopy of the microcirculation within the border zone of an Ostim® implant (asterisk) at day 6 after transfer onto the striated muscle tissue of the dorsal skinfold chamber. Note that there are only a few activated leukocytes adhering at the endothelium of postcapillary venules (arrows), indicating an adequate biocompatibility of the bone substitute. (A) Blue-light epi-illumination with contrast enhancement by 5% FITC-labeled dextran 150,000 i.v. for visualization of the microvasculature. (B) Green-light epi-illumination for visualization of rhodamine 6G-stained leukocytes. Scale bars: 170 μm.

J. Biomed. Mater. Res. Vol.9999, 9999 Pages: NA

View Normal Image View List of Images

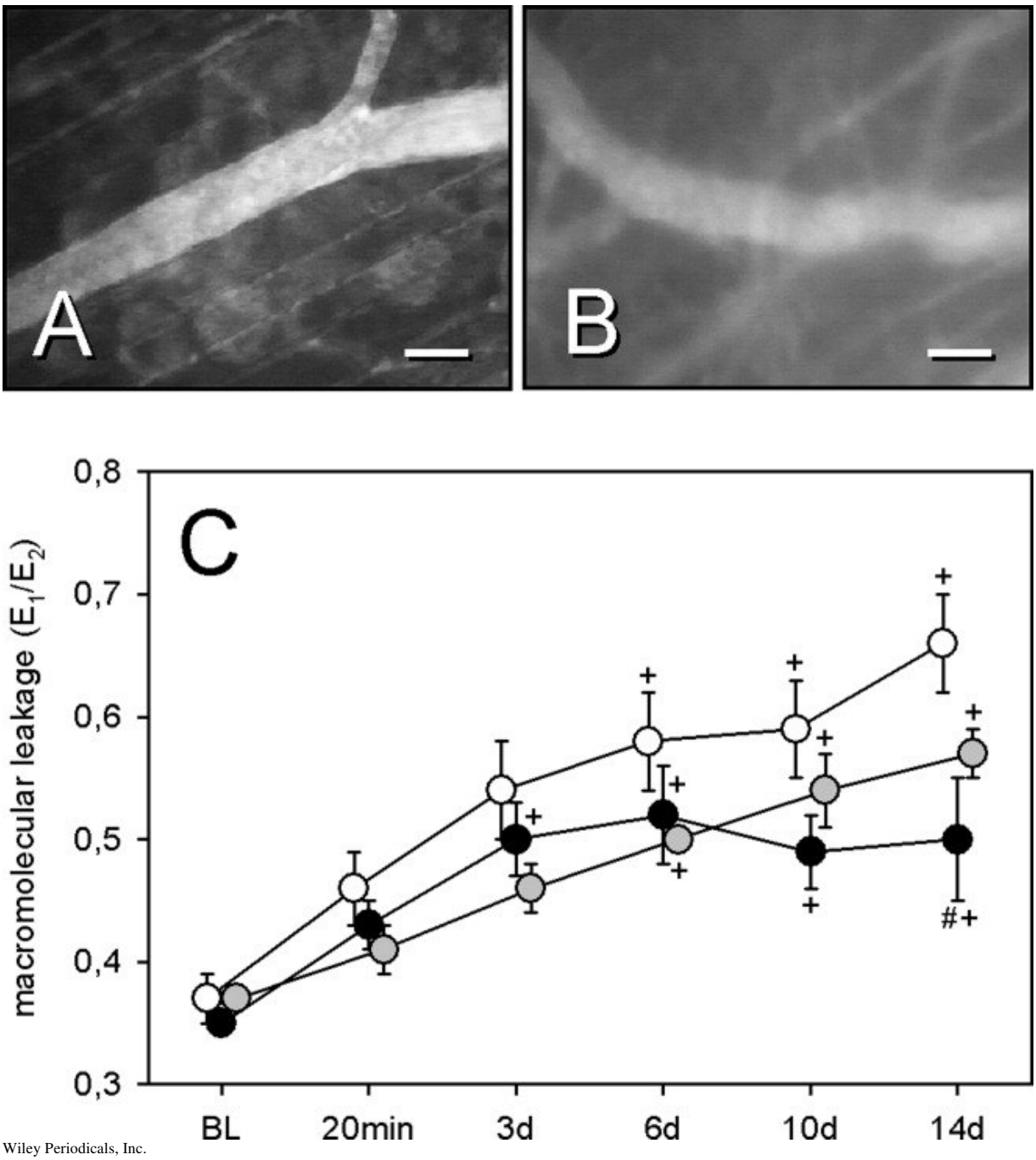

Figure 4. (A,B) Intravital fluorescence microscopy of postcapillary venules of the dorsal skinfold chamber preparation before implantation of cancellous bone (A, baseline) and at day 14 after implantation (B). Fourteen days after implantation of cancellous bone, extravasation of the intravenously injected macromolecular fluorescent dye FITC-labeled dextran 150,000 is increased, indicating an altered integrity of the endothelial cells lining the vessel walls. Blue-light epi-illumination with contrast enhancement by 5% FITC-labeled dextran 150,000 i.v. Scale bars: 50 μm. (C) Macromolecular leakage as a parameter of microvascular permeability of postcapillary and collecting venules within ROIs of the border zones of Ostim® (black circles), Cerabone® (grey circles), and cancellous bone (white circles) before (BL, baseline) as well as 20 min, 3, 6, 10, and 14 days after implantation into the dorsal skinfold chamber of Syrian golden hamsters. Mean ± SEM. $^{+}p < 0.05$ versus BL; $^{\#}p < 0.05$ versus cancellous bone at corresponding time points.

J. Biomed. Mater. Res. Vol.9999, 9999 Pages: NA

View Normal Image View List of Images

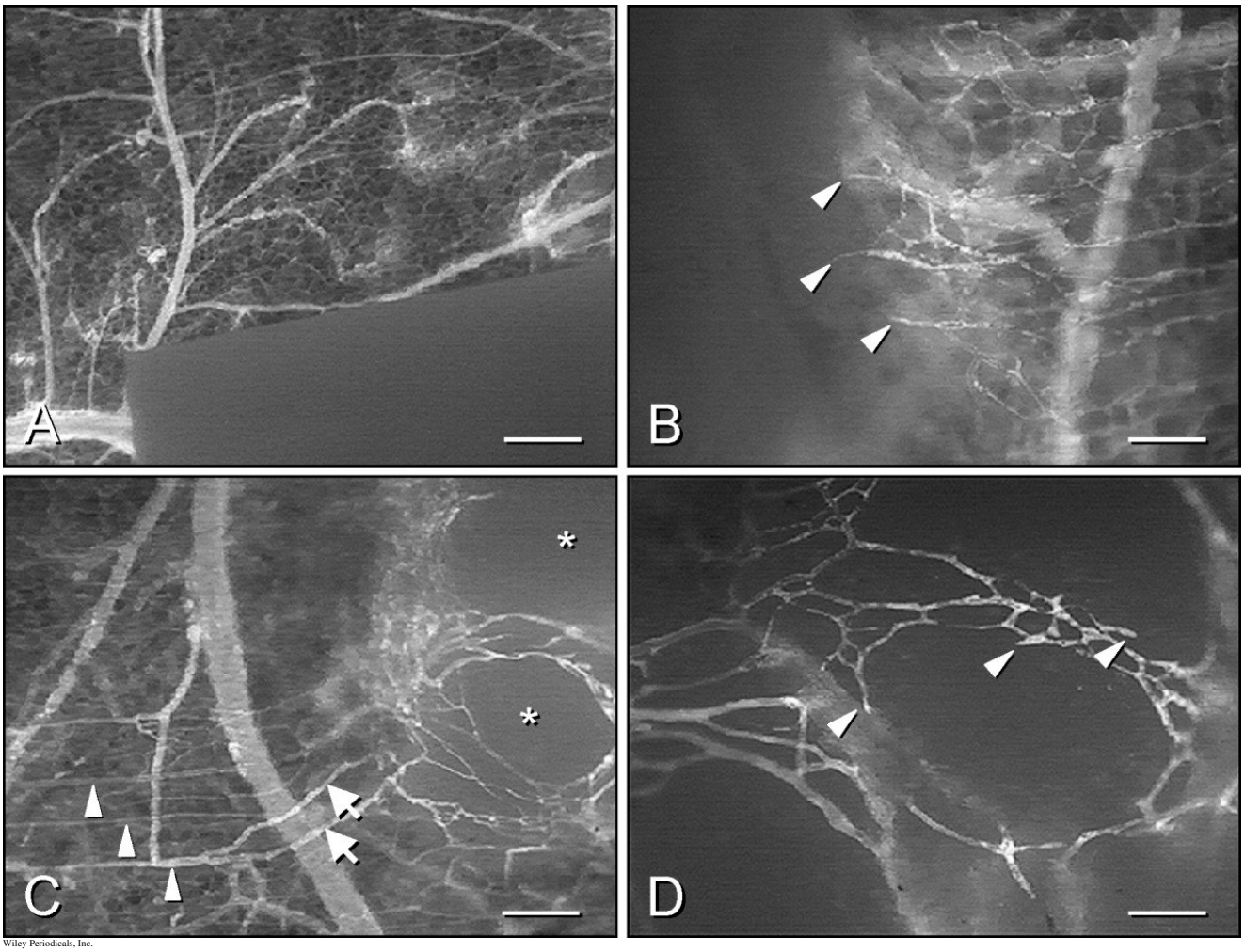

Figure 5. Intravital fluorescence microscopy of Ostim® at 20 min (A) as well as day 3 (B) and day 14 (C,D) after implantation into the dorsal skinfold chamber of a Syrian golden hamster. At day 3, first signs of angiogenesis can be observed in the border zone of the implant, characterized by capillary sprouts (B, arrow heads) ingrowing into the bone substitute. At day 14, the border zone of the implant is already well vascularized (C), while areas in the center of the implant still lack newly formed blood vessels (C, asterisks). However, higher magnification of the bone substitute demonstrates that the angiogenic process continues, as indicated by capillary sprouts (D, arrow heads) ingrowing into avascular areas of the center of the implant (D). Note that the newly formed microvascular network of the implant is drained by postcapillary vessels (C, arrows), which connect to the parallelly arranged striated muscle capillaries (C, arrow heads) of the skinfold chamber. Blue light epi-illumination with contrast enhancement by 5% FITC-labeled dextran 150,000 i.v. Scale bars: A = 270 μm; B = 105 μm; C = 170 μm; D = 105 μm.

J. Biomed. Mater. Res. Vol.9999, 9999 Pages: NA

View Normal Image View List of Images

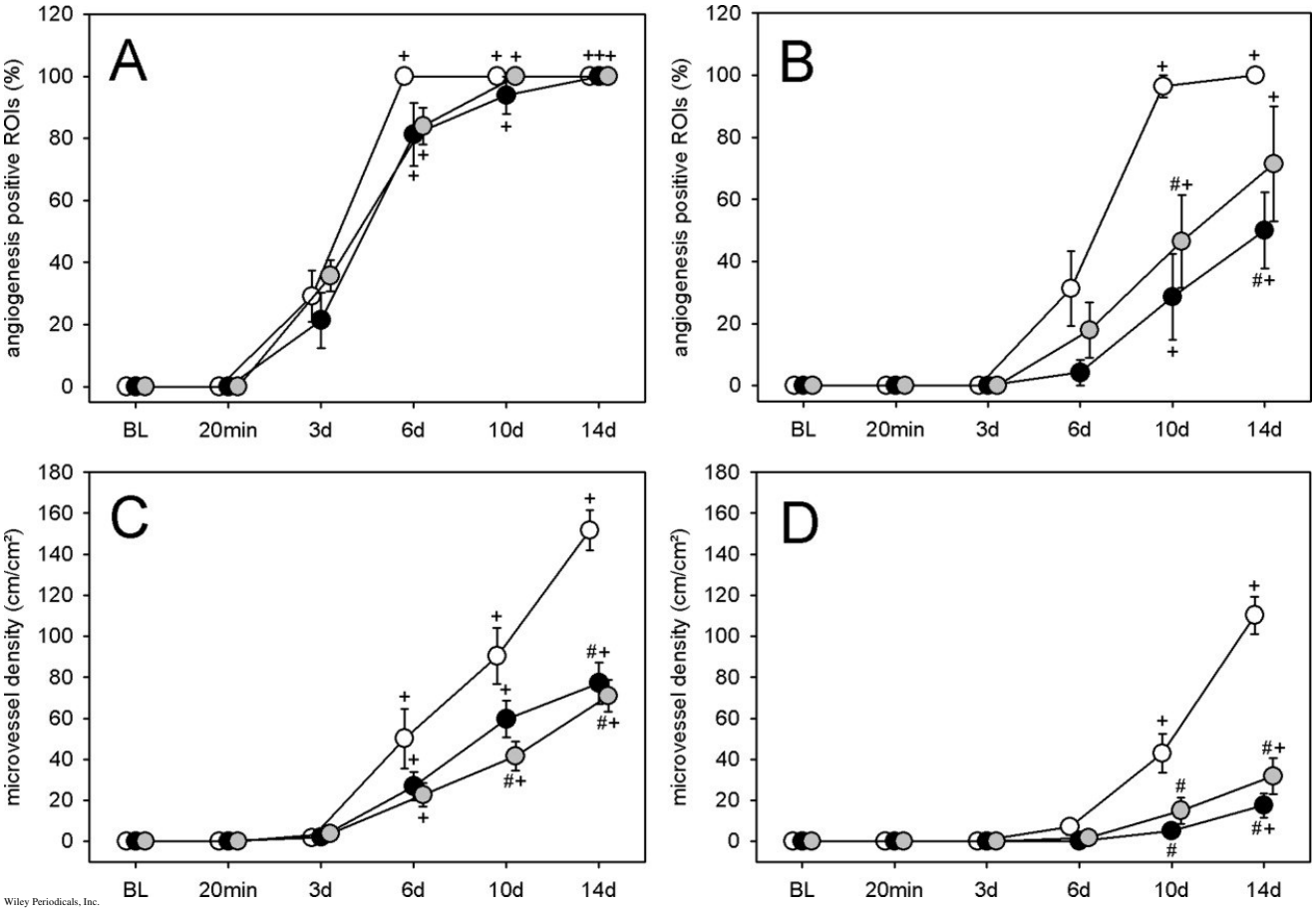

Figure 6. (A,B) Time course of angiogenesis after implantation of Ostim® (black circles), Cerabone® (grey circles), and cancellous bone (white circles) expressed as percentage of "angiogenesis positive" regions of interest (ROIs) within the border zone (A) and the center (B) of the implants before (BL, baseline) as well as 20 min, 3, 6, 10, and 14 days after implantation into the dorsal skinfold chamber of Syrian golden hamsters. ROIs were defined as "angiogenesis positive," when signs of blood vessel development, that is capillary buds and sprouts or newly formed microvessels, could be identified. (C,D) Quantitative assessment of the microvessel density, given as cm/cm^2, in ROIs within the border zone (C) and the center (D) of Ostim (black circles), Cerabone (grey circles), and cancellous bone (white circles) before (BL, baseline) as well as 20 min, 3, 6, 10, and 14 days after implantation into the dorsal skinfold chamber of Syrian golden hamsters. Mean ± SEM. $^{+}p < 0.05$ versus BL; $^{\#}p < 0.05$ versus cancellous bone at corresponding time points.

J. Biomed. Mater. Res. Vol.9999, 9999 Pages: NA

View Normal Image View List of Images

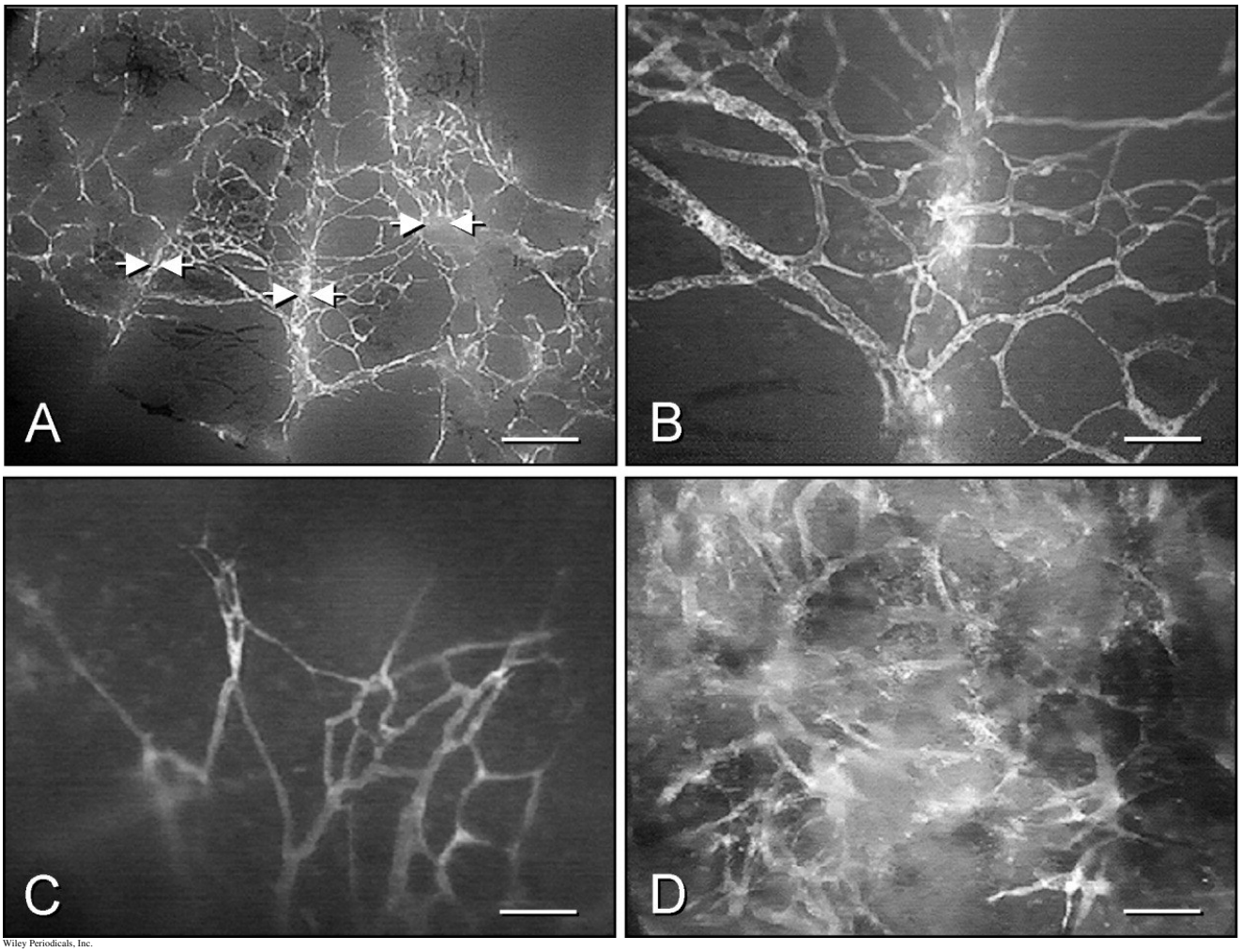

Figure 7. Intravital fluorescence microscopy of Ostim® (A,B), Cerabone® (C), and cancellous bone (D) at day 14 after implantation into the dorsal skinfold chamber of a Syrian golden hamster. The lower magnification of Ostim (A) displays areas of material degradation (arrows). The higher magnification of these areas (B) reveals a dense ingrowth of newly formed blood vessels through the biomaterial, creating microvascular networks surrounding the remaining nondegraded Ostim fragments. In contrast to Ostim, capillaries grow only over the surface of Cerabone (C), while the granulation tissue surrounding the fragments of isolated cancellous bone is pierced by many blood vessels (D). Blue light epi-illumination with contrast enhancement by 5% FITC-labeled dextran 150,000 i.v. Scale bars: A = 270 μm; B-D = 105 μm.

J. Biomed. Mater. Res. Vol.9999, 9999 Pages: NA

View Normal Image View List of Images

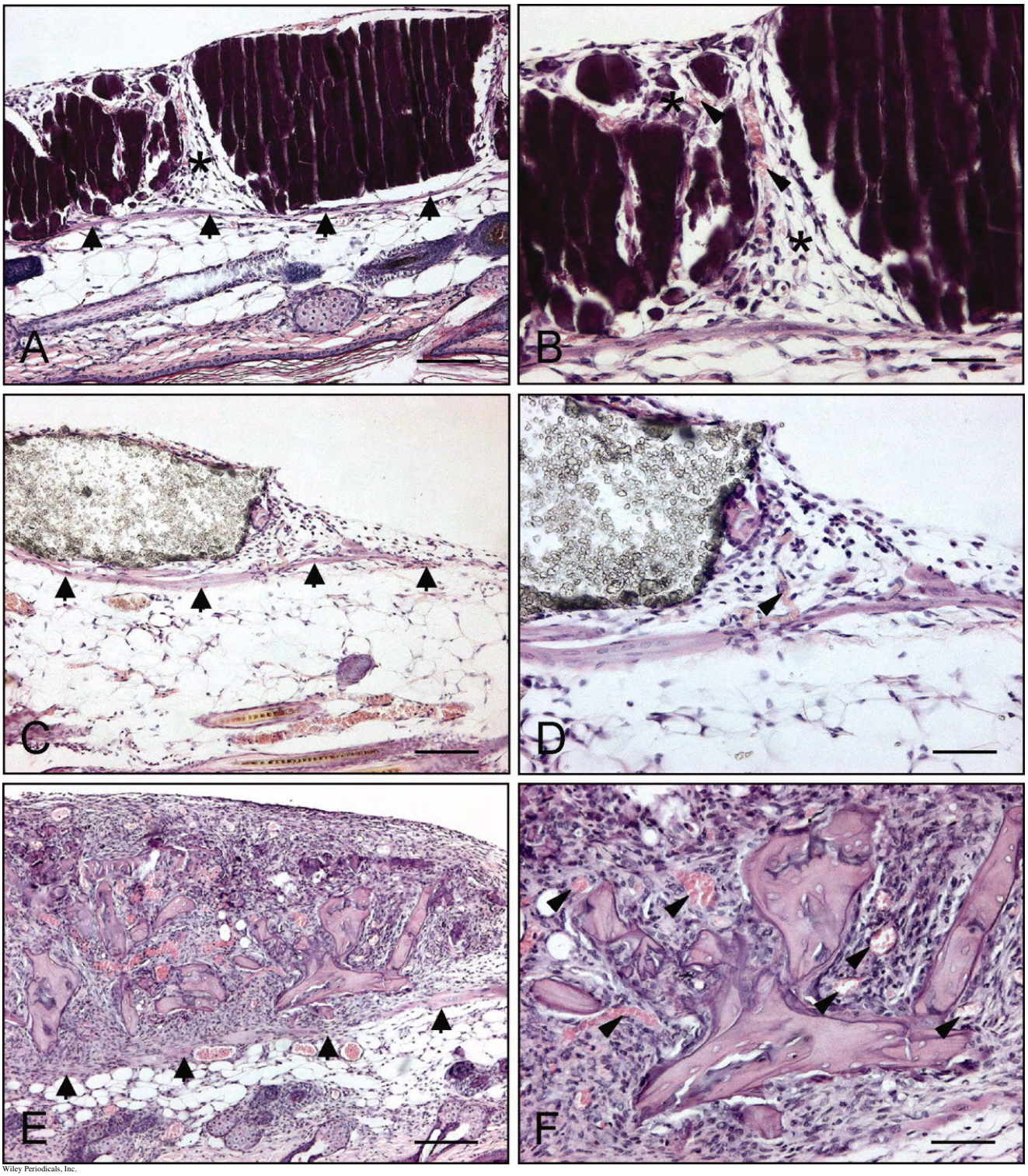

Figure 8. Hematoxylin-eosin stained cross sections of Ostim® (A), Cerabone® (C), and cancellous bone (E) at day 14 after implantation onto the striated muscle tissue (arrows) of the dorsal skinfold chamber. Higher magnification reveals the formation of granulation tissue with newly developed blood vessels (arrow heads) surrounding the Ostim (B), Cerabone (D), and cancellous bone implants (F). In contrast to Cerabone, Ostim exhibits areas of degradation (asterisks), where blood vessels can directly invade the biomaterial (A,B). Cancellous bone is surrounded by a richly vascularized granulation tissue with an increased microvessel density and a higher cellular content, when compared with the synthetic bone substitutes Ostim and Cerabone. Scale bars: A,C = 110 μm; E = 170 μm; B,D,F = 55 μm. [Color figure can be viewed in the online issue, which is available at www.interscience.wiley.com.]

J. Biomed. Mater. Res. Vol.9999, 9999 Pages: NA

View Normal Image View List of Images

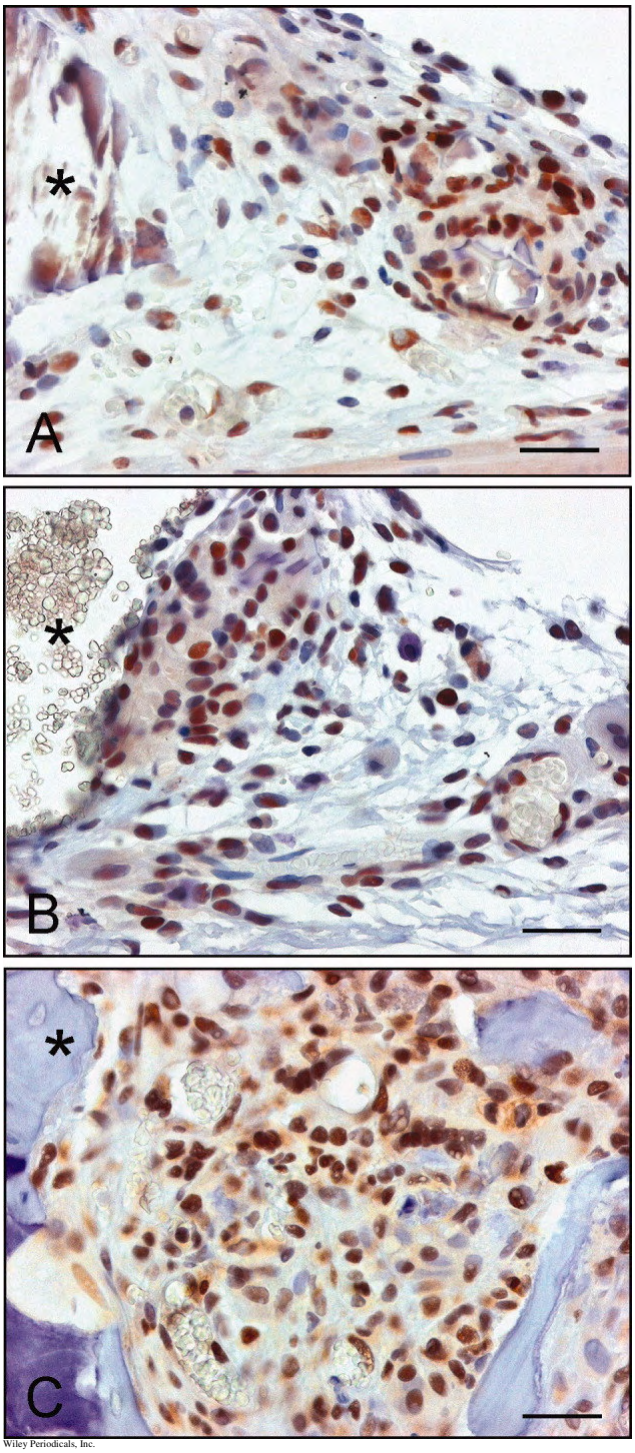

Figure 9. Immunohistochemical detection of PCNA-positive cells within the granulation tissue surrounding Ostim® (A, asterisk), Cerabone® (B, asterisk), and cancellous bone (C, asterisk) at day 14 after implantation into the dorsal skinfold chamber. Note that in the major fraction of cells surrounding Ostim and Cerabone positive PCNA staining can be observed (A,B). In cancellous bone almost all cells surrounding the implant show proliferative activity (C). Scale bars: A-C = 25 μm. [Color figure can be viewed in the online issue, which is available at www.interscience.wiley.com.]